

## Laser butt welding of thin stainless steel 316L sheets in asymmetric configurations: A numerical study

Ebrahimi, Amin; Hermans, Marcel J.M.

**DOI**

[10.1016/j.jajp.2023.100154](https://doi.org/10.1016/j.jajp.2023.100154)

**Publication date**

2023

**Document Version**

Final published version

**Published in**

Journal of Advanced Joining Processes

**Citation (APA)**

Ebrahimi, A., & Hermans, M. J. M. (2023). Laser butt welding of thin stainless steel 316L sheets in asymmetric configurations: A numerical study. *Journal of Advanced Joining Processes*, 8, Article 100154. <https://doi.org/10.1016/j.jajp.2023.100154>

**Important note**

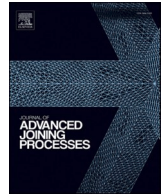
To cite this publication, please use the final published version (if applicable). Please check the document version above.

**Copyright**

Other than for strictly personal use, it is not permitted to download, forward or distribute the text or part of it, without the consent of the author(s) and/or copyright holder(s), unless the work is under an open content license such as Creative Commons.

**Takedown policy**

Please contact us and provide details if you believe this document breaches copyrights. We will remove access to the work immediately and investigate your claim.



## Laser butt welding of thin stainless steel 316L sheets in asymmetric configurations: A numerical study

Amin Ebrahimi<sup>\*</sup>, Marcel J.M. Hermans

Department of Materials Science and Engineering, Faculty of Mechanical, Maritime and Materials Engineering, Delft University of Technology, Mekelweg 2, Delft 2628CD, The Netherlands

### ARTICLE INFO

#### Keywords:

Laser welding  
Thin metal plates  
Misalignment  
Asymmetric configurations  
Numerical simulation  
Heat and fluid flow modelling

### ABSTRACT

Laser butt welding of thin metal sheets is a widely used fusion-based joining technique in industrial manufacturing. A comprehensive understanding of the complex transport phenomena during the welding process is essential for achieving high-quality welds. In the present work, high-fidelity numerical simulations are employed to investigate the influence of various symmetric and asymmetric welding configurations on the melt-pool behaviour in conduction-mode laser butt welding of stainless steel sheets. The analysis focuses on the effects of laser power density, heat source misplacement and different welding scenarios, including plates with a root gap, high-low mismatches, and dissimilar thicknesses, on the molten metal flow and heat transfer. The results show that advection is the dominant mechanism for energy transfer in the melt pool, and its contribution increases with higher laser power. The non-uniform temperature distribution over the melt-pool surface induces Marangoni shear forces, driving the flow of molten metal and leading to the formation of vortices and periodic flow oscillations within the pool. The effects of various types of asymmetries on the thermal and molten metal flow fields, as well as the process stability, are thoroughly examined and compared with symmetrical welding configurations. These comprehensive simulations provide valuable insights into the fluid flow dynamics and thermal field evolution during laser butt welding of thin metal sheets. The knowledge gained from this study can facilitate process optimisation and guide the improvement of weld quality in practical applications.

### Introduction

Asymmetry in laser butt welding is prevalent in industrial manufacturing and often results from misalignment of workpieces (Tang et al., 2023), misplacement of the heat source (*i.e.* uneven distribution of heat input) (Andrews and Nicol, 1981), and dissimilarities in plate thicknesses (Li et al., 2020) or material compositions (Ai et al., 2022; Flint et al., 2021). Such an asymmetry can alter the complex heat and fluid flow during welding, which in turn can affect the melt-pool shape, process stability and quality of the joints (DebRoy and David, 1995). However, correct control of the workpieces assembly and the welding set-up is usually challenging in practice, particularly for thin sheets (plate thickness < 1 mm) (Chen et al., 2022; Walther et al., 2022). Hence, a better understanding of heat and fluid flow during welding is essential to control the process adequately, determine welding parameter tolerances, and achieve desired joint properties with a reduced number of defects.

In laser welding, the material absorbs thermal energy from a laser

beam and heats up locally above its melting temperature. This results in the formation of a melt pool that solidifies subsequently, creating a permanent joint. The control of laser welding processes primarily relies on maintaining a delicate balance between the thermal energy absorbed from the laser beam and the thermal energy dissipated to the surroundings and within the material (Zhou and Tsai, 2005). However, heat transfer in welding is a complex phenomenon involving multiple mechanisms such as conduction, advection, and radiation (Lancaster, 1986), and depends on various factors including the physical properties of the material, the geometrical configuration of the workpieces, and process parameters such as power density, welding speed, and characteristics of the laser system (Ayoola et al., 2017; Baruah and Bag, 2017; Chludzinski et al., 2021; Ebrahimi et al., 2021c; 2022). Moreover, the interaction between the laser and the material, as well as the presence of unsteady molten metal flow, solid-liquid phase transformations, and moving boundaries of the melt pool, further complicate heat transfer in fusion welding. Analytical methods often lack sufficient accuracy in predicting thermal and fluid flow fields in welding, and rarely provide

<sup>\*</sup> Corresponding author.

E-mail address: [A.Ebrahimi@tudelft.nl](mailto:A.Ebrahimi@tudelft.nl) (A. Ebrahimi).

<https://doi.org/10.1016/j.jajp.2023.100154>

Received 20 July 2023; Received in revised form 14 August 2023; Accepted 17 August 2023

Available online 19 August 2023

2666-3309/© 2023 The Authors. Published by Elsevier B.V. This is an open access article under the CC BY license (<http://creativecommons.org/licenses/by/4.0/>).

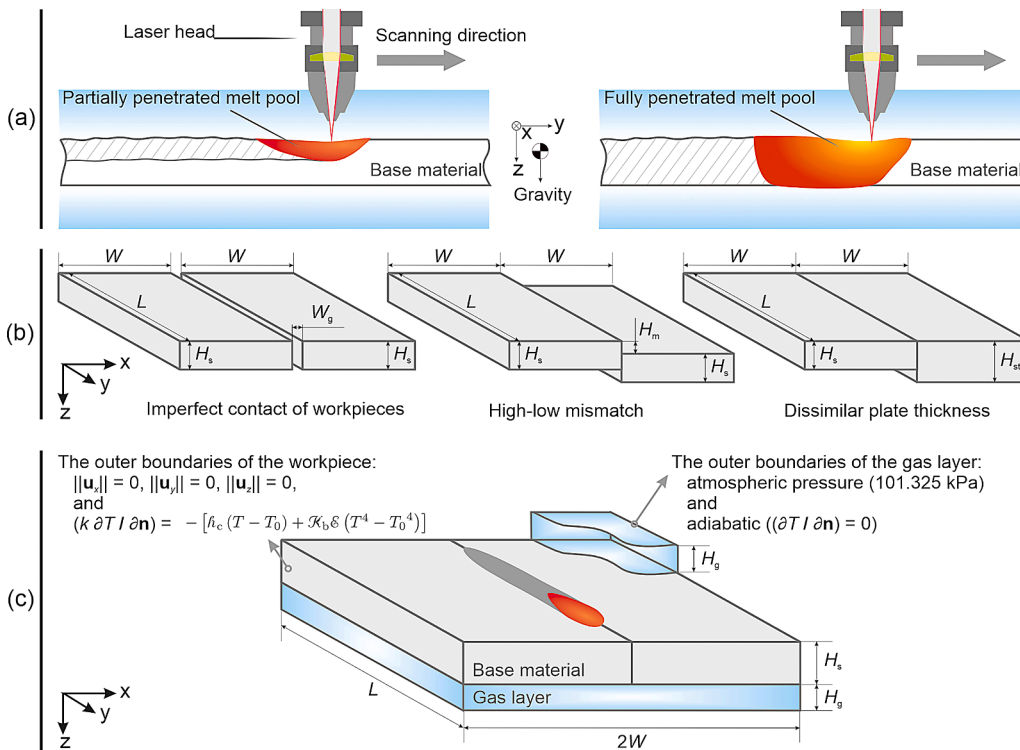


**Fig. 1.** Schematic of laser butt welding, dimensional parameters and the boundary conditions employed in numerical simulations. (a) longitudinal cross-section of the melt pool for partially penetrated (left) and fully penetrated (right) conditions, (b) different geometrical configurations studied in the present work, and (c) a representation of the computational domain and the boundary conditions prescribed on the outer boundaries. The computational domain is defined in a Cartesian coordinate system, and the thickness  $H_s$ , width  $W$  and length  $L$  of the plate are  $500 \mu$ ,  $3.5 \text{ mm}$  and  $13 \text{ mm}$  respectively. The height of the gas layer  $H_g$  is  $1 \text{ mm}$ . Part of the gas layer is clipped in sub-figure (c) for visualisation.

reasonable solutions for complex welding scenarios (Zhou and Tsai, 2005). Experimental approaches face numerous challenges in detecting thermal and fluid flow fields during welding due to high temperatures, dynamic molten metal flow, opacity, and the small size of the melt pool (Aucott et al., 2018), and can be prohibitively expensive for exploring design possibilities. Physics-based numerical simulations offer a viable alternative by providing reasonably accurate representations of thermal and fluid flow fields in welding. They present an opportunity to reduce costs associated with experiments (Cook and Murphy, 2020; Ebrahimi et al., 2021a; 2021b; 2021d) and contribute to the realisation of the goals of 'Industry 4.0' (De Pond et al., 2020).

The majority of previous studies on numerical simulations of fusion-based butt welding focus on symmetrical configurations (Chukkan et al., 2015; Patterson et al., 2021; Tsirkas et al., 2003; Xu et al., 2019; Zhang et al., 2020). Numerical investigations of asymmetric butt welding generally address situations involving dissimilar material properties (Hejripour et al., 2019; Li et al., 2022; Liang and Luo, 2017; Wei et al., 2015) or plate thicknesses (Kholoud and Akbari, 2021; Li et al., 2020; Xia and Jin, 2016; Zhang et al., 2019). To date, little attention has been paid to other types of asymmetric configurations that arise due to misalignment of workpieces, misplacement of the heat source and imperfect contact of workpieces; however studies have revealed that these asymmetries can significantly impact the quality of butt welds (Andrews, 1996; Ferreira and Branco, 1991; Lotsberg, 2009; Xiao et al., 2021). Moreover, previous studies commonly neglect the influence of internal flow behaviour during welding and incorporate its effect on energy transfer by introducing calibration parameters into the model (Lindgren and Lundbäck, 2018), limiting the general applicability of these models in predicting thermal and fluid flow fields in different welding scenarios (Ebrahimi, 2022). A major drawback of using calibration parameters is that their values are not known *a priori* and require tuning for each specific welding situation. This is due to the non-linear response of convection in fusion welding to changes in process parameters, material properties, and operating conditions (Ebrahimi et al., 2019a). Convection plays a substantial role in energy transfer during

fusion welding and additive manufacturing (DebRoy and David, 1995; Wei et al., 2021) of metallic materials. Hence, ignoring its effect can adversely affect the accuracy and reliability of numerical simulations. Further studies are needed to enhance the current understanding of internal flow behaviour and heat transfer in asymmetric welding configurations.

The present study focuses on the characterization of thermal and fluid flow fields in conduction-mode laser butt welding of metal sheets. The objective is to examine the influence of various asymmetric configurations including workpiece misalignment, heat-source misplacement, and imperfect workpiece contact, on the heat flow and weld bead profile in laser butt welding with different laser power densities. To achieve this, high-fidelity physics-based numerical simulations are employed to predict and analyse the complex and transient transport phenomena that occur during laser butt welding. The specific emphasis of this study is on conduction-mode laser welding due to its widespread use in achieving high-quality joints in thin metal sheets. The simulations in this study take into account the influence of intricate and transient laser-matter interactions, such as the effects of surface temperature and morphology on laser absorptivity, using an enhanced laser-beam absorption model (Ebrahimi et al., 2022).

## Methods

The influence of different asymmetric configurations, shown schematically in Fig. 1, on conduction-mode laser butt welding of stainless steel (AISI 316L) sheets is studied numerically in the present work. An Yb:YAG fibre transmissible laser with an emission wavelength ( $\lambda$ ) of  $1.030 \mu\text{m}$ , a spot diameter ( $D4\sigma$ ) of  $1 \text{ mm}$  and a Gaussian intensity profile is employed to locally melt the metal sheets that are initially at an ambient temperature of  $T_i = 300 \text{ K}$ . The laser beam is aligned with the  $z$ -axis and is perpendicular to the sheet surface. The travel speed ( $\mathcal{V}$ ) is set to  $10 \text{ mm}^{-1}$  and three different laser powers ( $\mathcal{P}$ ) of  $200 \text{ W}$ ,  $250 \text{ W}$  and  $350 \text{ W}$  are studied. Argon shielding gas is employed to protect the melt pool from oxidation. In the simulations, two layers of argon gas

**Table 1**

Summary of the parameters studied in the present work.  $H_s$  is  $500 \mu$  for all the cases studied in the present work. In symmetrical welding configurations with perfect contact, the value of  $W_g$  is  $0 \mu$ .

Parameter	Imperfect contact	High-low mismatch	Dissimilar plate thickness
$W_g$ [ $\mu\text{m}$ ]	100	–	–
$H_m$ [ $\mu\text{m}$ ]	–	100, 250	–
$H_{st}$ [ $\mu\text{m}$ ]	–	–	600, 750
Laser beam position along the x-axis, $x_b$ [ $\mu\text{m}$ ]	0, +100, +250	0, +100, +250, – 100, – 250	0, +100, +250, – 100, – 250

above and below the sheets with a height of  $H_g = 1 \text{ mm}$  were included to track the deformations of the melt-pool surface. For each configuration shown in Fig. 1(b), several additional cases are considered in which the laser beam is misplaced intentionally to study its effect on the melt pool evolution. Details of the geometrical parameters used to define the problem are presented in Fig. 1 and Table 1. In total, 72 cases are studied in the present work.

High-fidelity physics-based numerical simulations were constructed on the basis of our previous computational model (Ebrahimi et al., 2021c; 2022) that has a generic foundation and is able to predict essential features of conduction-mode laser welding such as heat and fluid flow, solid-liquid phase transformation, melt-pool surface oscillations, and variations in laser absorptivity due to changes in surface morphology and temperature. The model has been developed based on the finite-volume approach within the framework of a proprietary solver, ANSYS Fluent (Release 19.2), and is described in detail and validated rigorously elsewhere (Ebrahimi, 2022; Ebrahimi et al., 2022). Here, the model is leveraged to explain the physics of heat and fluid flow in laser butt welding. The volume-of-fluid (VOF) method (Hirt and Nichols, 1981) was employed in the model to track the motion of the

melt-pool surface. The source and sink terms in the momentum and energy equations, and the laser absorptivity and surface tension models were implemented by employing user-defined functions programmed in the C programming language. Laser absorptivity is a system parameter and its value is influenced by several factors, including the composition of the base material, surface temperature, laser beam incident angle, shielding gas efficiency, and characteristics of the laser system (Ebrahimi et al., 2022; Kromer et al., 2023; Ye et al., 2019). An enhanced model that takes these factors into account was utilised in the present work to determine the laser absorptivity during the process, obviating the need for calibrating the value of absorptivity in the simulations. The enhanced absorptivity model is described in detail in our previous work (Ebrahimi et al., 2022). The molten metal and the shielding gas are assumed to be Newtonian fluids and their densities do not change with pressure. Accordingly, the governing conservation equations for mass, momentum, energy and the scalar function  $\phi$ , which represents the local volume-fraction of the metal phase in a computational cell, are defined as follows:

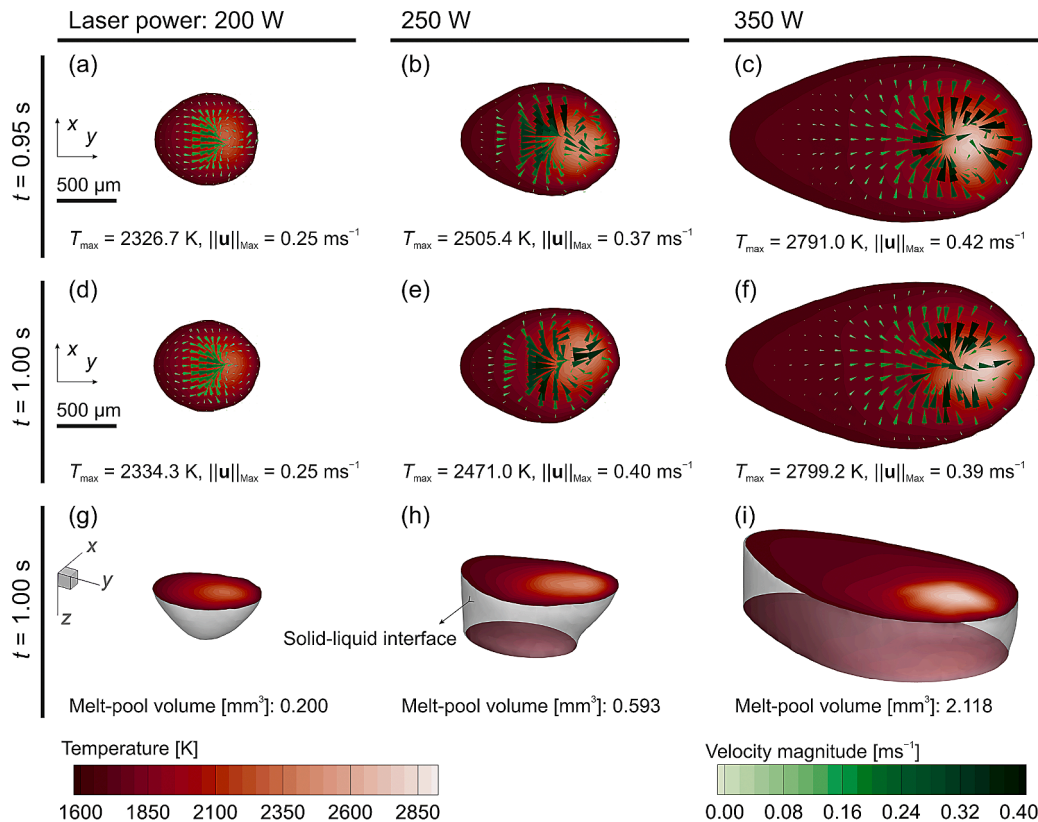


**Fig. 2.** Numerically predicted melt-pool shapes, and thermal and fluid flow fields over the melt-pool surface for different laser powers. The plates are in a symmetrical configuration (*i.e.*  $x_b = 0 \mu\text{m}$ ) and have perfect thermal contact.  $x_b$  is the laser beam position along the x-axis.

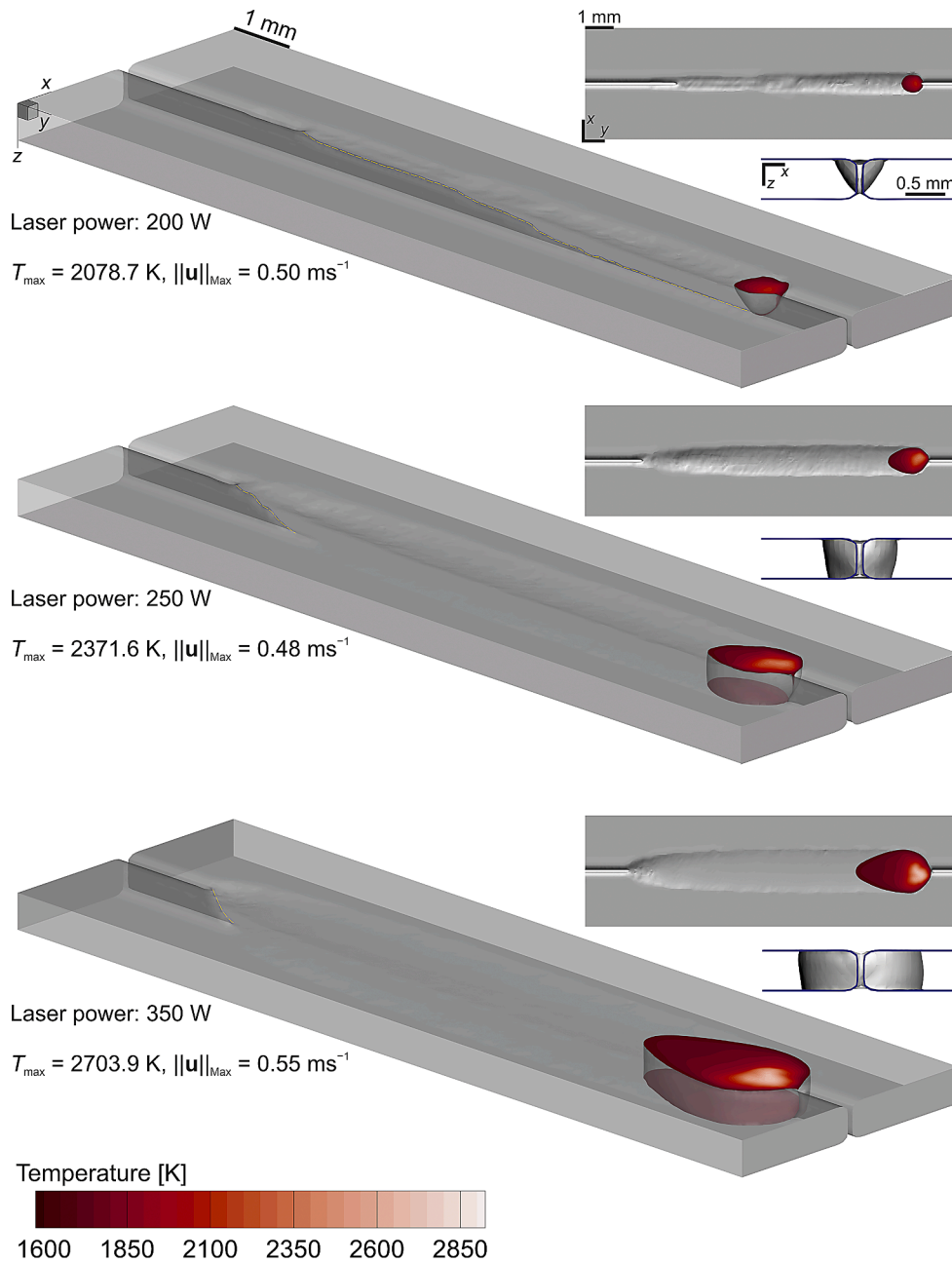


**Fig. 3.** Numerically predicted weld bead, melt-pool shape, and temperature distribution over the melt-pool surface for different laser powers at  $t = 1 \text{ s}$ . The results were obtained for welding of metal sheets with a root gap of  $W_g = 100 \mu\text{m}$  in a symmetric configuration (*i.e.*  $x_b = 0 \mu\text{m}$ ).

$$\frac{D\rho}{Dt} + \rho(\nabla \cdot \mathbf{u}) = 0, \quad (1)$$

$$\rho \frac{D\mathbf{u}}{Dt} = \mu \nabla^2 \mathbf{u} - \nabla p - C \frac{(1-\psi)^2}{\psi^3 + \epsilon} \mathbf{u} + \mathbf{F}_s, \quad (2)$$

$$\rho \frac{Dh}{Dt} = \frac{k}{c_p} \nabla^2 h - \rho \frac{D(\psi \mathcal{L}_f)}{Dt} + S_q + S_l, \quad (3)$$

$$\frac{D\phi}{Dt} = 0. \quad (4)$$

Here,  $t$  is the time,  $\mathbf{u}$  the fluid velocity vector,  $\rho$  the density,  $p$  the pressure,  $\mu$  the dynamic viscosity,  $c_p$  the specific heat capacity,  $k$  the thermal conductivity,  $h$  the sensible heat,  $\mathcal{L}_f$  the latent heat of fusion,  $\psi$

the local liquid volume-fraction,  $(\psi \mathcal{L}_f)$  the latent heat,  $C$  the mushy-zone constant, equal to  $10^7 \text{ kg m}^{-2} \text{ s}^{-2}$  (Ebrahimi et al., 2019b), and  $\epsilon$  a constant incorporated to avoid division by zero, equal to  $10^{-3}$ . Forces acting on the melt-pool surface (*i.e.* surface tension force, Marangoni shear force and recoil pressure) are incorporated into the model by adding the source term  $\mathbf{F}_s$  to the momentum Eq. (2) (Ebrahimi et al., 2021c). The source term  $S_q$  is added to the energy Eq. (3) to model the thermal energy input from the laser beam (Ebrahimi et al., 2022). Heat losses from the base material due to radiation, convection and vaporisation are accounted for by adding the sink term  $S_l$  to the energy equation (Ebrahimi et al., 2022).

Thermo-physical properties of AISI 316L are considered to be temperature-dependent and are adopted from Ebrahimi et al. (2022). Accordingly, the effects of thermal buoyancy force are taken into

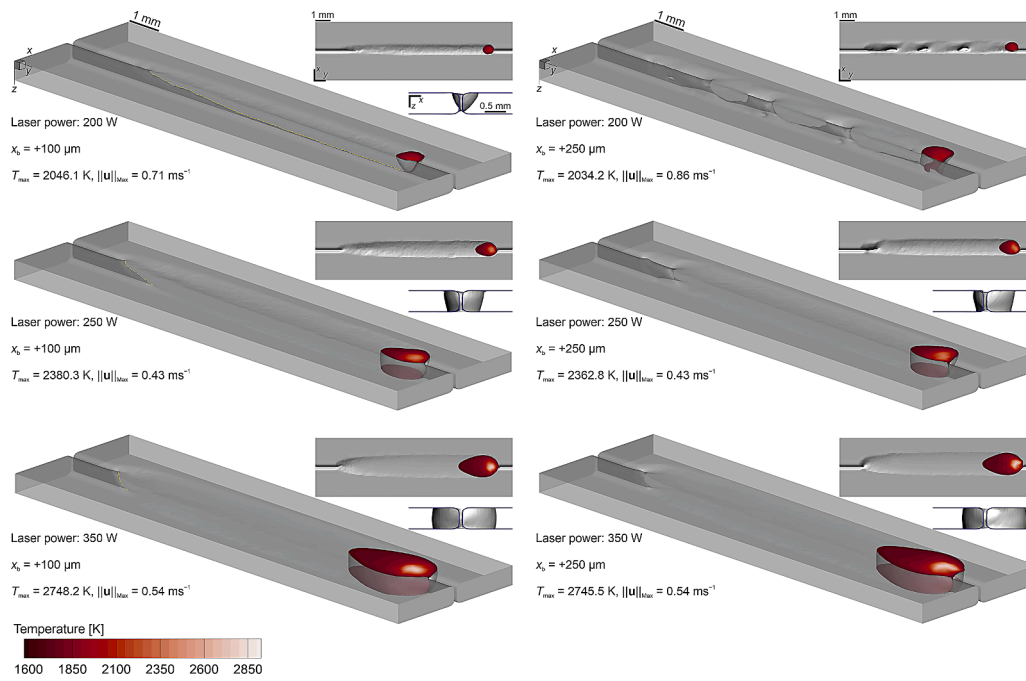


Fig. 4. Numerically predicted weld bead, melt-pool shape, and temperature distribution over the melt-pool surface for different laser powers at  $t = 1$  s. The results were obtained for welding of metal sheets with a root gap of  $W_g = 100 \mu\text{m}$  in an asymmetric configuration ( $x_b = 100 \mu\text{m}$  and  $250 \mu\text{m}$ ).

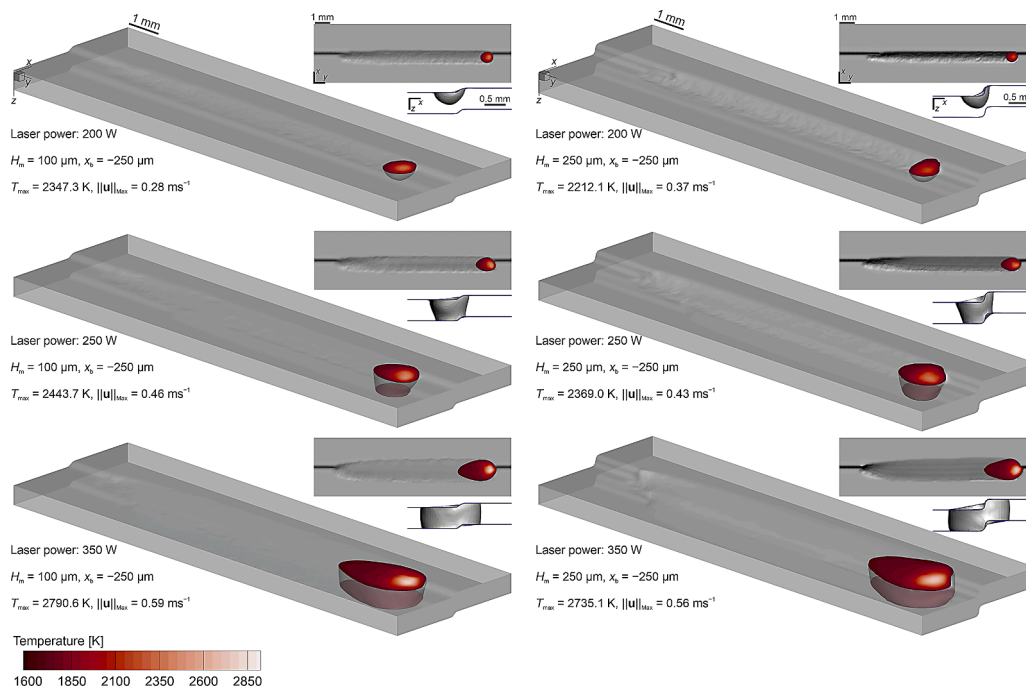
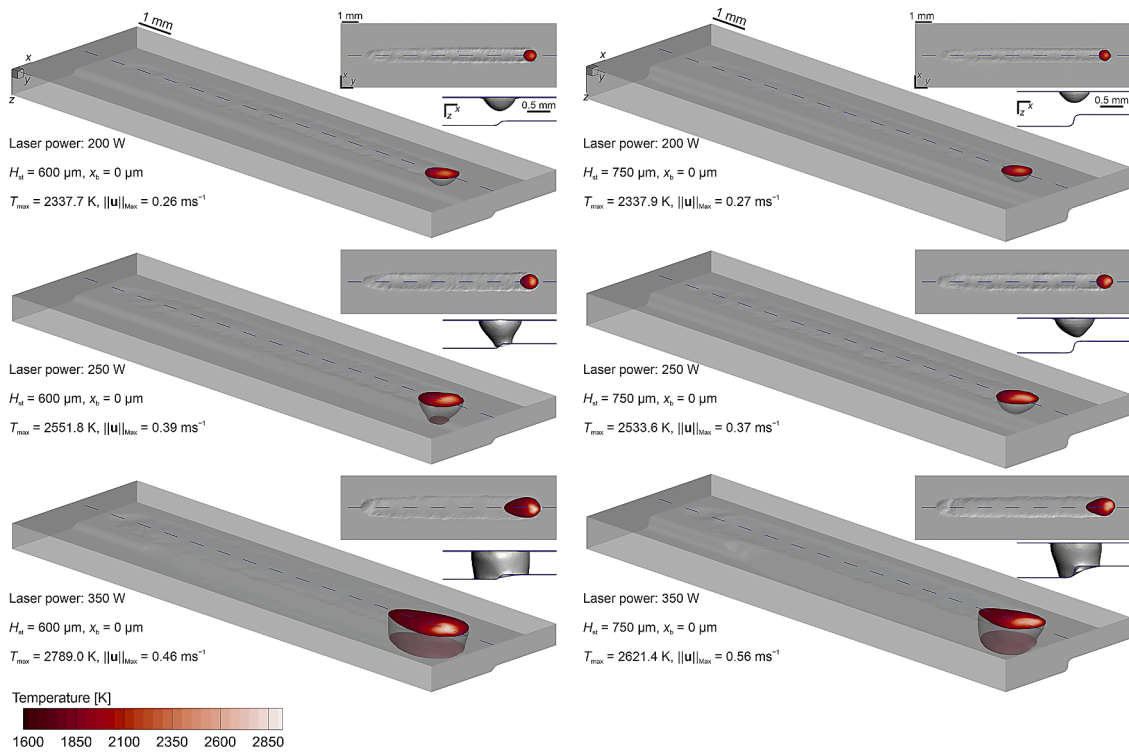


Fig. 5. Numerically predicted weld bead, melt-pool shape, and temperature distribution over the melt-pool surface for different laser powers at  $t = 1$  s. The results were obtained for welding of metal sheets with a high-low mismatch. Left column:  $H_m = 100 \mu\text{m}$ , and right column:  $H_m = 250 \mu\text{m}$ . The laser beam scans the centerline ( $x_b = 0 \mu\text{m}$ ).



**Fig. 6.** Numerically predicted weld bead, melt-pool shape, and temperature distribution over the melt-pool surface for different laser powers at  $t = 1$  s. The results were obtained for welding of metal sheets with dissimilar thicknesses. Left column:  $H_{st} = 600 \mu\text{m}$ , and right column:  $H_{st} = 750 \mu\text{m}$ . The laser beam scans the centreline ( $x_b = 0 \mu\text{m}$ ). The dashed blue line indicates the boundary between the metal sheets before welding.

account using a temperature-dependent density model in the present simulations. Thermal conductivity, viscosity and density of argon are small compared to those of AISI 316L, and their variations with temperature are generally negligible during conduction-mode laser welding (Ebrahimi, 2022). Thus, the physical properties of argon are assumed to be constant and the values are taken from Ebrahimi et al. (2022), Jaques (1988). In each computational cell, the effective material properties are computed as follows:

$$\xi = \phi \xi_m + (1 - \phi) \xi_g, \quad (5)$$

where,  $\xi$  corresponds to density  $\rho$ , viscosity  $\mu$ , thermal conductivity  $k$  or specific heat capacity  $c_p$ , and subscripts 'm' and 'g' indicate metal or gas respectively.

The computational grid consists of about  $1.5 \times 10^6$  hexahedral cells with minimum cell spacing of  $25 \mu\text{m}$  that results in about 35 cells along the melt-pool width, which is demonstrably sufficient to achieve grid-independent results (Ebrahimi, 2022; Ebrahimi et al., 2021c). Spatial and temporal discretisation were performed employing the second-order central differencing scheme and a first-order implicit scheme respectively. The advection of the scalar field  $\phi$  was formulated using an explicit compressive VOF method (Ubbink, 1997). The coupling between velocity and pressure fields was resolved employing the PISO (pressure-implicit with splitting of operators) scheme (Issa, 1986), and the pressure interpolation was performed using the PRESTO (pressure staggering option) scheme (Patankar, 1980). A fixed time-step size of  $\Delta t = 2 \mu\text{s}$  was chosen, resulting in a Courant number ( $\text{Co} = \|u\| \Delta t / \Delta x$ ) less than 0.3. Simulations were executed in parallel employing 16 cores (AMD EPYC 7452) for each simulation, leading to a run-time ranging between 50 to 135 h. The validity of the present model in predicting heat and fluid flow in laser melting is meticulously investigated by comparing the numerical predictions with experimental, numerical and analytical data, and are reported in our previous works (Ebrahimi, 2022; Ebrahimi et al., 2019a; 2021c; 2022).

## Results and discussion

### Melt-pool behaviour in symmetrical welding configurations with perfect contact

Figure 2 shows the numerical results of the transient thermal and fluid flow analysis for different laser powers when welding metal sheets in a symmetrical configuration with perfect contact. The figure presents snapshots of the temperature and velocity fields over the melt-pool surface at two different time instances after reaching the quasi-steady-state condition, and the predicted melt-pool shapes. The high energy density of the laser beam causes localized heating of the plates, resulting in the formation of a melt pool. The main mechanisms of heat transfer in this process are convection within the melt pool and conduction through the surrounding solid material. Approximately 3% of the energy absorbed by the material from the laser beam is lost from the plates due to heat dissipation by convection and radiation. As shown in Fig. 2, increasing the laser power  $\mathcal{P}$  leads to an increase in the melt-pool depth. For  $\mathcal{P} = 200$  W, the melt-pool depth does not reach the plate thickness, and a partially-penetrated pool is formed. However, for  $\mathcal{P} = 250$  W and 350 W, full penetration is achieved.

The temperature distribution over the melt-pool surface leads to local changes in molten metal surface tension, resulting in the generation of the Marangoni shear force. The molten metal flow in conduction-mode laser welding is primarily driven by the Marangoni shear force, where surface tension gradients over the melt-pool surface drive flow towards regions of higher surface tension. The molten metal surface tension is affected by its chemical composition and the presence of surface active elements such as sulphur, oxygen, selenium and tellurium. The results indicate an inward flow over the surface, which is ascribed to the enhancement of molten metal surface tension due to an increase in the surface temperature. The interaction between the fluid flowing from the front part of the pool toward the rear with the opposing flow from the rear part results in the formation of a pair of vortices on the pool

surface, causing a periodic flow oscillation. An increase in the energy input to the material results in an increase in the peak temperature and the melt-pool volume. For temperatures above the critical temperature ( $T_c \approx 1610\text{ K}$ ), the surface tension decreases with a further increase in the temperature, leading to the formation of an outward fluid motion. Fluid flow oscillations due to the interaction between vortices on the surface, and flow instabilities that emerge in the vicinity of the laser spot centre, due to interactions between the inward and outward flows, result in a complex unsteady flow pattern in the pool that is inherently three-dimensional.

Analysis of the numerically predicted thermal and fluid flow fields shows that advection is the primary mechanism for energy transfer in melt pools during laser welding of metallic sheets, as evidenced by Péclet numbers ( $Pe = \rho c_p \mathcal{S} \|\mathbf{u}\| / k$ ) of approximately 40 (for a laser power of  $\mathcal{S} = 200\text{ W}$ ), 80 (for a laser power of  $\mathcal{S} = 250\text{ W}$ ), and 110 (for a laser power of  $\mathcal{S} = 350\text{ W}$ ). The results suggest that the contribution of advection to the total energy transfer in the pool increases with increasing the energy input to the material. This is attributed to the enhancement of the magnitude of temperature gradients and, hence, the Marangoni shear forces generated on the surface of the melt pool.

#### Welding of metal sheets with a root gap

The weld bead, melt-pool shape, and the temperature distribution over the melt-pool surface for different laser powers at  $t = 1\text{ s}$  are shown in Fig. 3. These results were obtained from numerical simulations of welding metal sheets with a root gap in a symmetric configuration ( $x_b = 0\ \mu\text{m}$ , where  $x_b$  is the laser beam position along the  $x$ -axis). As the temperature rises locally due to the laser heat input, the initial melting occurs at the edges of the plates. The molten metal gradually accumulates and forms a liquid bridge that connects the plates. Upon cooling, the liquid bridge solidifies and creates a joint between the plates. The predicted fluid flow field shows that the molten metal flow pattern in welding metal sheets with a root gap resembles that in welding metal sheets with perfect contact with similar laser powers after reaching the quasi-steady state. The presence of a gap between the plates results in a lower amount of laser energy absorbed by the plates compared to the cases with perfect contact. Hence, joint formation and attainment of the maximum melt-pool width are delayed after the process initiation. This delay decreases with increasing the laser power. Once the plates melt and a liquid bridge forms between them, the amount of laser energy absorbed by the plates increases and becomes comparable to that in the case of perfect contact. However, a lower amount of laser energy is absorbed by the plates, and a lower peak temperature is observed over the melt-pool surface compared to the case of perfect contact. This is because the front part of the laser beam scans regions where the gap exists.

The thermal field generated in the plates and consequently the melting behaviour and process stability are influenced by the location of the heat source. Figure 4 shows the effects of heat source location on the weld bead, melt-pool shape, and the temperature distribution over the melt-pool surface for different laser powers at  $t = 1\text{ s}$ . Joint formation and attainment of the maximum melt-pool width occur earlier when the heat source is placed  $100\ \mu\text{m}$  away from the centreline than in welding of plates with a root gap in a symmetric configuration (see Fig. 3). This can be attributed to the fact that less laser energy is lost through the gap when the centre of the laser beam with a Gaussian intensity profile is located on one of the plates, resulting in rapid melting of the plate and formation of a liquid bridge between the plates. The difference between the weld bead appearances obtained in welding metal sheets with a root gap in a symmetric configuration ( $x_b = 0\ \mu\text{m}$ ) and asymmetric configuration ( $x_b = 100\ \mu\text{m}$ ) are found to become insignificant with increasing the laser power.

Displacing the laser beam further away from the centreline to a distance of  $x_b = 250\ \mu\text{m}$  results in significant melting of one of the plates. The edge of one of the plates undergoes significant melting, primarily influenced by the surface tension exerted by the molten metal at the plate's periphery. Thus, the edge transforms into a semi-cylindrical shape. As the volume of the molten metal gradually increases during welding, a liquid bridge forms that joins the plates. When employing a laser power of  $200\text{ W}$ , the volume of molten metal is limited and the molten metal flow is unstable, resulting in periodic perforations during the welding process. Increasing the laser power increases the volume of molten metal, thereby establishing a more stable liquid bridge between the plates.

#### Welding of metal sheets with a high-low mismatch

The weld bead geometry, the shape of the melt pool, and the temperature distribution on the melt-pool surface at are presented in Fig. 5 for different laser powers. These results were obtained by numerically simulating the welding process of metal sheets with high-low mismatches of 20% and 50% of the plate thickness, and the laser beam was assumed to scan along the centreline ( $x_b = 0\ \mu\text{m}$ ) of the metal sheets. The melt pool surface forms an angle with the horizontal plane when there is a high-low mismatch between the plates, and the melt-pool depth increases in the same direction accordingly. The laser beam incident angle is slightly increased by the inclination of the melt pool surface, but this increase in the incident angle is insignificant (less than  $40^\circ$ ) to cause a notable change in the laser absorptivity for the cases studied in the present work. However, plate positioning influences the contact area between the plates, affecting the thermal field evolution in the plates. For thin metal sheets, where the melt-pool size is comparable to the plate thickness, the thermal field generated in the plates causes the melt-pool depth to grow towards the bottom surface of the higher plate, as shown in Fig. 5 for a laser power of  $200\text{ W}$ . The effective plate thickness beneath the laser beam is reduced by an increase in the high-low mismatch, and thus the melt pool can reach the bottom surface of the higher plate. The thermal field generated in the plates and the melt pool shape evolution are affected by the displacement of the laser beam from the centreline. The effects of heat source location on the weld bead, melt-pool shape, and the temperature distribution over the melt-pool surface for different laser powers when welding metal sheets with a high-low mismatch are presented in Appendix 'The effects of heat source location in welding metal sheets with a high-low mismatch'.

#### Welding of metal sheets with dissimilar thicknesses

The weld bead, melt-pool shape, and temperature distribution over the melt-pool surface for various laser powers at  $t = 1\text{ s}$  are depicted in Fig. 6. These results were derived from numerical simulations of butt welding of metal sheets with dissimilar thicknesses, assuming that the laser beam scans the metal sheets' centreline ( $x_b = 0\ \mu\text{m}$ ). The melt-pool size decreases with increasing plate thickness due to the enhanced cooling effect resulting from the increased heat diffusion to the surrounding material. This results in a higher cooling rate in the thick plate than in the thin plate, and thus the melt pool develops towards the thinner plate. This observation is consistent with the experimental measurements of thermal field and melt-pool shape during laser butt welding of Ti6Al4V sheets with dissimilar thicknesses reported by Li et al. (2020). The plate thickness has negligible influence on the peak temperature and molten metal velocity, particularly for low laser powers. A comparison of the results obtained for welding with a laser power of  $250\text{ W}$  shows that full penetration is attainable when the difference between the plate thicknesses is approximately 10%. However, when the difference in plate thickness exceeds 10%, a higher laser power

is required to achieve full penetration. Displacing the laser beam notably influences the development of the melt pool and thus the joint quality, as shown in Figs. A.3 and A.4 in appendix ‘The effects of heat source location in welding metal sheets with a dissimilar thicknesses’.

## Conclusions

The influence of various symmetric and asymmetric welding configurations on the melt-pool behaviour in conduction-mode laser butt welding of stainless steel sheets was studied using high-fidelity numerical simulations. The simulations have incorporated detailed models for heat transfer, solid-liquid phase transformation, and melt-pool dynamics, as well as an enhanced laser-beam absorption model that takes into account the effects of surface temperature and morphology on local laser absorptivity. The analysis has focused on the effects of laser power density, heat source misplacement and different welding scenarios involving root gaps, high-low thickness mismatches, and dissimilar plate thicknesses on the molten metal flow and heat transfer during welding. The main findings of this study are:

- Advection is the dominant mechanism for energy transfer in the melt pool, and its contribution increases with increasing laser power.
- The temperature distribution over the melt-pool surface creates local variations in molten metal surface tension, generating the Marangoni shear force that drives the molten metal flow and leads to the formation of vortices and periodic flow oscillations within the pool.
- The presence of a gap between the plates reduces the amount of laser energy absorbed by the plates and delays joint formation and maximum melt-pool width. However, once a liquid bridge forms between the plates, the amount of laser energy absorbed by the plates increases and becomes comparable to perfect contact.
- The displacement of the laser beam from the centreline affects the thermal field evolution and melt pool shape. Displacing the laser beam slightly towards one of the plates in welding of thin plates with a root gap results in rapid melting of the plate and liquid bridge formation. Displacing the laser beam further away from the centreline results in significant melting of one of the plates and can lead to the formation of periodic perforation during welding with low laser powers.
- The high-low mismatch between the plates causes the melt-pool surface to form an angle with the horizontal plane and influences the direction along which the melt pool grows. The thermal field evolution causes the melt pool depth to grow towards the bottom surface of the higher plate.
- The melt-pool size decreases with increasing plate thickness due to enhanced cooling resulting from increased heat diffusion to the surrounding material. The melt pool develops towards the thinner plate when welding plates of dissimilar thicknesses.

These comprehensive simulations provide valuable insights into the fluid flow dynamics and thermal field evolution during laser butt welding of thin metal plates. The results reveal how different asymmetric configurations affect the melt-pool shape, process stability and

## Appendix A

### *The effects of heat source location in welding metal sheets with a high-low mismatch*

Numerical simulations of welding metal sheets with high-low mismatches of 20% and 50% of the plate thickness were performed for different laser powers. The weld bead geometry, the melt-pool shape, and the melt-pool surface temperature at  $t = 1$  s are shown in Figs. A.1 and A.2 for the cases where the laser beam centre was on the lower plate ( $x_b = -250 \mu\text{m}$ ) and the higher plate ( $x_b = 250 \mu\text{m}$ ), respectively. These results demonstrate the effect of displacing the laser beam from the centreline in welding thin plates with a high-low mismatch.

joint quality. The knowledge gained from this study can facilitate process optimisation, determining welding parameter tolerances, and guide the improvement of weld quality in practical applications by enabling better control of the workpiece assembly, the welding set-up, and the laser parameters.

The present model can serve as a basis for future research by extending it to incorporate the effects of arc plasma, metal vapour, shielding gas, and electromagnetic phenomena in electric arc-based fusion welding processes. This extension would provide a more comprehensive understanding of heat and mass transfer during welding. Moreover, the impact of asymmetric configurations on the microstructure and mechanical properties of the welds can be investigated through metallurgical analysis and mechanical testing of the welded specimens. Insights into the relationship between welding parameters, asymmetry, and the resulting weld properties can be offered by correlating these results with the predicted thermal and fluid flow fields from numerical simulations.

## CRediT authorship contribution statement

**Amin Ebrahimi:** Conceptualization, Methodology, Software, Validation, Formal analysis, Investigation, Resources, Project administration, Data curation, Visualization, Writing – original draft, Writing – review & editing. **Marcel J.M. Hermans:** Funding acquisition, Resources, Writing – review & editing.

## Declaration of Competing Interest

The authors declare that they have no known competing financial interests or personal relationships that could have appeared to influence the work reported in this paper.

## Data availability

The raw/processed data required to reproduce these findings cannot be shared at this time due to their large size, but representative samples of the research data are presented in the paper. Other datasets generated during this study are available from the corresponding author on reasonable request.

## Acknowledgment

This research was carried out under project numbers F31.7.13504 and S17024h in the framework of the Partnership Program of the Materials innovation institute M2i ([www.m2i.nl](http://www.m2i.nl)) and the Foundation for Fundamental Research on Matter (FOM) ([www.fom.nl](http://www.fom.nl)), which is part of the Netherlands Organisation for Scientific Research ([www.nwo.nl](http://www.nwo.nl)). This research project is also a part of Aim2XL program ([www.m2i.nl/aim2xl](http://www.m2i.nl/aim2xl)). The authors would like to extend their gratitude to Dr. Ian M. Richardson, from the IR Welding Consultancy, for valuable discussions during the preparation of this article.

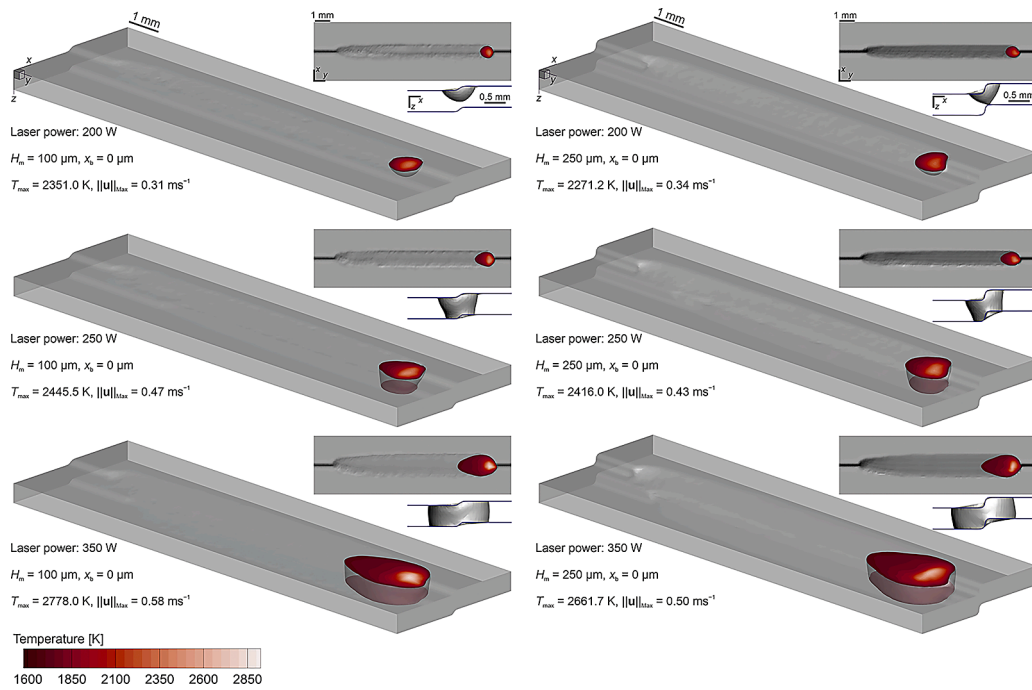


**Fig. A.1.** Numerically predicted weld bead, melt-pool shape, and temperature distribution over the melt-pool surface for different laser powers at  $t = 1$  s. The results were obtained for welding of metal sheets with a high-low mismatch. Left column:  $H_m = 100 \mu\text{m}$ , and right column:  $H_m = 250 \mu\text{m}$ . The centre of the laser beam is located on the lower plate ( $x_b = -250 \mu\text{m}$ ).

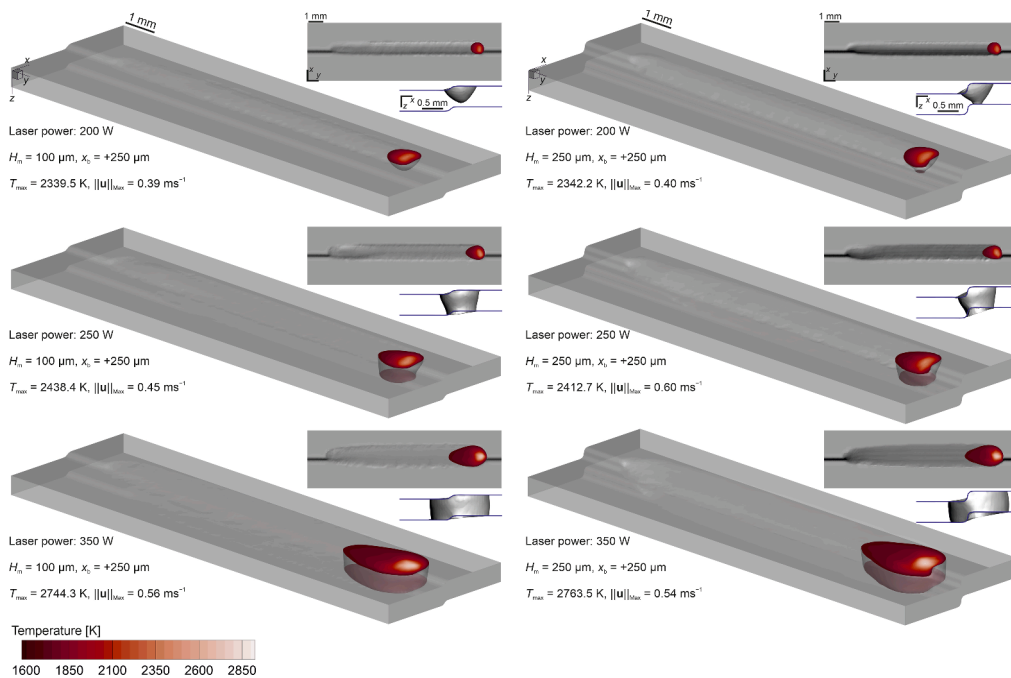


**Fig. A.2.** Numerically predicted weld bead, melt-pool shape, and temperature distribution over the melt-pool surface for different laser powers at  $t = 1$  s. The results were obtained for welding of metal sheets with a high-low mismatch. Left column:  $H_m = 100 \mu\text{m}$ , and right column:  $H_m = 250 \mu\text{m}$ . The centre of the laser beam is located on the higher plate ( $x_b = +250 \mu\text{m}$ ).

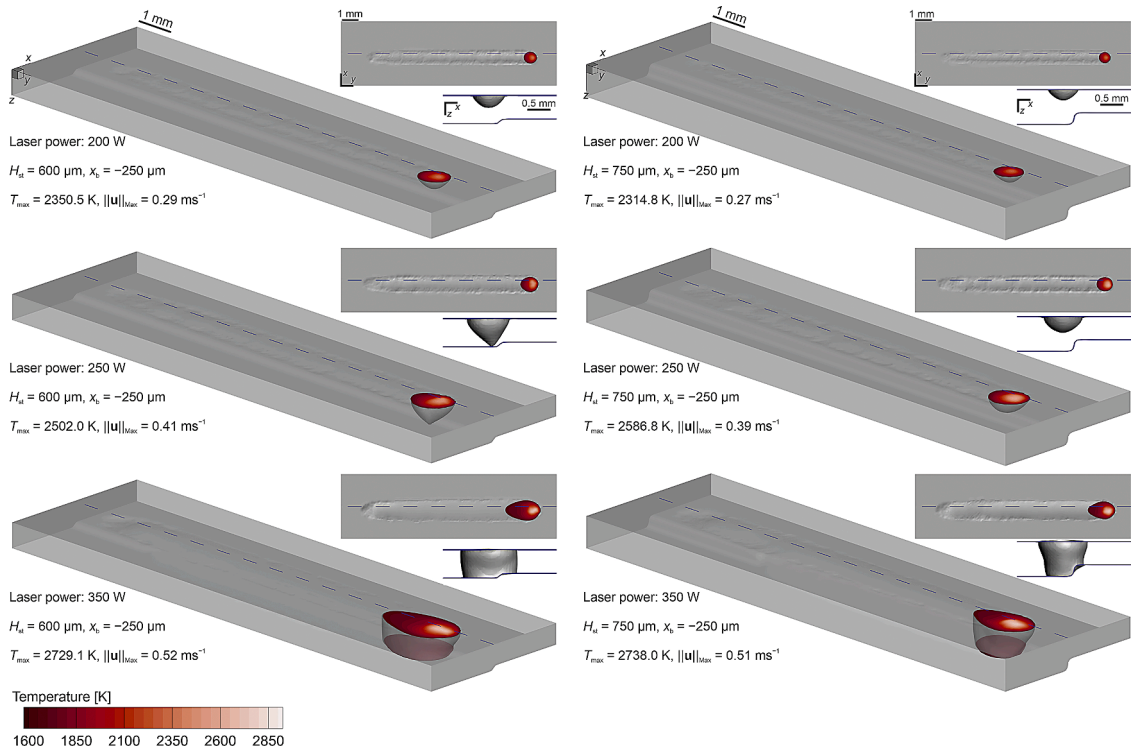


**Fig. A.3.** Numerically predicted weld bead, melt-pool shape, and temperature distribution over the melt-pool surface for different laser powers at  $t = 1$  s. The results were obtained for welding of metal sheets with dissimilar thicknesses. Left column:  $H_{st} = 600 \mu\text{m}$ , and right column:  $H_{st} = 750 \mu\text{m}$ . The centre of the laser beam is located on the thicker plate ( $x_b = -250 \mu\text{m}$ ). The dashed blue line indicates the boundary between the metal sheets before welding.

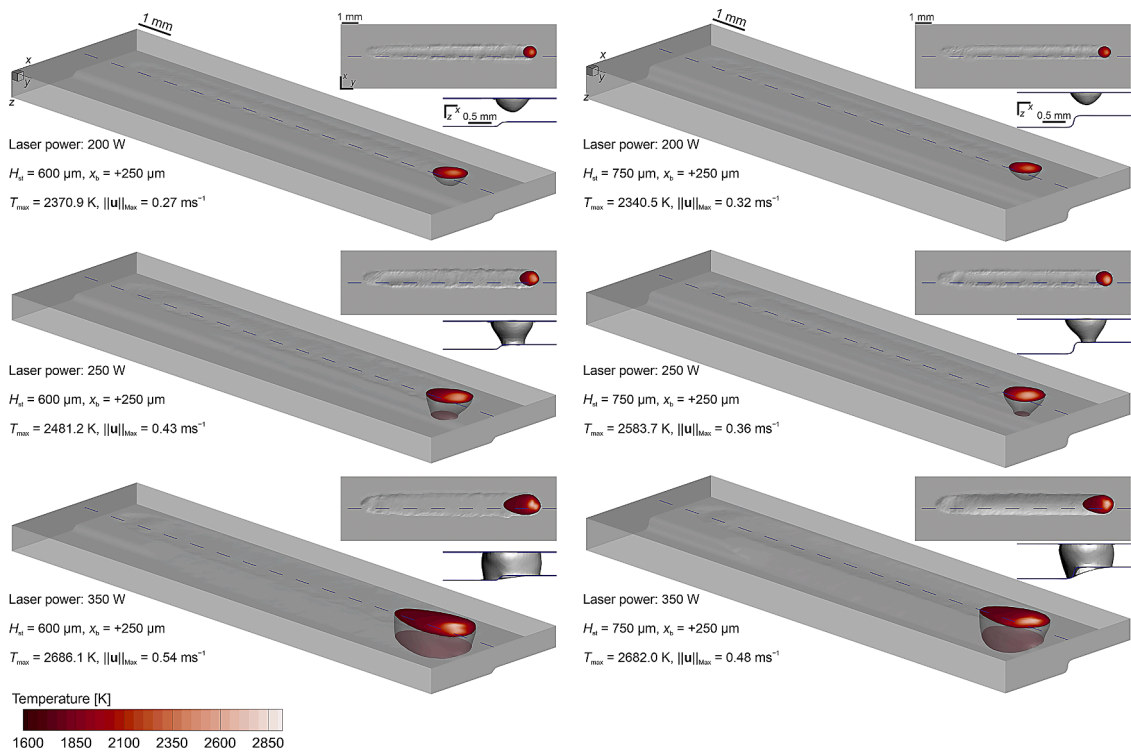


**Fig. A.4.** Numerically predicted weld bead, melt-pool shape, and temperature distribution over the melt-pool surface for different laser powers at  $t = 1$  s. The results were obtained for welding of metal sheets with dissimilar thicknesses. Left column:  $H_{st} = 600 \mu\text{m}$ , and right column:  $H_{st} = 750 \mu\text{m}$ . The centre of the laser beam is located on the thinner plate ( $x_b = +250 \mu\text{m}$ ). The dashed blue line indicates the boundary between the metal sheets before welding.

## The effects of heat source location in welding metal sheets with a dissimilar thicknesses

Numerical simulations of welding metal sheets with dissimilar thicknesses were performed for different laser powers. The thickness of one of the plates was increased by 20% and 50% of the plate thickness  $H_s$  that is 500  $\mu\text{m}$ . The weld bead geometry, the melt-pool shape, and the melt-pool surface temperature at  $t = 1\text{ s}$  are shown in Figure for the cases where the laser beam centre was on the thicker plate ( $x_b = -250\ \mu\text{m}$ ) and the thinner plate ( $x_b = 250\ \mu\text{m}$ ), respectively. These results demonstrate the effect of displacing the laser beam from the centreline in welding thin plates with dissimilar thicknesses.

## References

- Ai, Y., Liu, X., Huang, Y., Yu, L., 2022. The analysis of asymmetry characteristics during the fiber laser welding of dissimilar materials by numerical simulation. *Int. J. Adv. Manuf. Technol.* <https://doi.org/10.1007/s00170-021-08312-8>.
- Andrews, J.G., Nicol, D.A.C., 1981. Asymmetric heat flow in welding. *Q. J. Mech. Appl. Math.* 34 (2), 203–211. <https://doi.org/10.1093/qjmam/34.2.203>.
- Andrews, R.M., 1996. The effect of misalignment on the fatigue strength of welded cruciform joints. *Fatigue Fract. Eng. Mater. Struct.* 19 (6), 755–768. <https://doi.org/10.1111/j.1460-2695.1996.tb01320.x>.
- Aucott, L., Dong, H., Mirihanage, W., Atwood, R., Kidess, A., Gao, S., Wen, S., Marsden, J., Feng, S., Tong, M., Connolly, T., Drakopoulos, M., Kleijn, C.R., Richardson, I.M., Browne, D.J., Mathiesen, R.H., Atkinson, H.V., 2018. Revealing internal flow behaviour in arc welding and additive manufacturing of metals. *Nat. Commun.* 9 (1) <https://doi.org/10.1038/s41467-018-07900-9>.
- Ayoola, W., Suder, W., Williams, S., 2017. Parameters controlling weld bead profile in conduction laser welding. *J. Mater. Process. Technol.* 249, 522–530. <https://doi.org/10.1016/j.jmatprot.2017.06.026>.
- Baruah, M., Bag, S., 2017. Influence of pulsation in thermo-mechanical analysis on laser micro-welding of Ti6Al4V alloy. *Opt. Laser Technol.* 90, 40–51. <https://doi.org/10.1016/j.optlastec.2016.11.006>.
- Chen, J., Ouyang, Z., Du, X., Wei, Y., 2022. Weld pool dynamics and joining mechanism in pulse wave laser beam welding of Ti-6Al-4V titanium alloy sheets assembled in butt joint with an air gap. *Opt. Laser Technol.* 146, 107558. <https://doi.org/10.1016/j.optlastec.2021.107558>.
- Chludzinski, M., dos Santos, R.E., Churiaque, C., Fernández-Vidal, S.R., Ortega-Iguña, M., Sánchez-Amaya, J.M., 2021. Pulsed laser butt welding of AISI 1005 steel thin plates. *Opt. Laser Technol.* 134, 106583. <https://doi.org/10.1016/j.optlastec.2020.106583>.
- Chukkan, J.R., Vasudevan, M., Muthukumar, S., Kumar, R.R., Chandrasekar, N., 2015. Simulation of laser butt welding of AISI 316L stainless steel sheet using various heat sources and experimental validation. *J. Mater. Process. Technol.* 219, 48–59. <https://doi.org/10.1016/j.jmatprot.2014.12.008>.
- Cook, P.S., Murphy, A.B., 2020. Simulation of melt pool behaviour during additive manufacturing: Underlying physics and progress. *Addit. Manuf.* 31, 100909. <https://doi.org/10.1016/j.addma.2019.100909>.
- De Pond, P.J., Fuller, J.C., Khairallah, S.A., Angus, J.R., Guss, G., Matthews, M.J., Martin, A.A., 2020. Laser-metal interaction dynamics during additive manufacturing resolved by detection of thermally-induced electron emission. *Commun. Mater.* 1 (1) <https://doi.org/10.1038/s43246-020-00094-y>.
- DeRoy, T., David, S.A., 1995. Physical processes in fusion welding. *Rev. Mod. Phys.* 67 (1), 85–112. <https://doi.org/10.1103/revmodphys.67.85>.
- Ebrahimi, A., 2022. Molten metal oscillatory behaviour in advanced fusion-based manufacturing processes. PhD dissertation. Delft University of Technology, Delft, The Netherlands.
- Ebrahimi, A., Babu, A., Kleijn, C.R., Hermans, M.J.M., Richardson, I.M., 2021. The effect of groove shape on molten metal flow behaviour in gas metal arc welding. *Materials* 14 (23), 7444. <https://doi.org/10.3390/ma14237444>.
- Ebrahimi, A., Kleijn, C.R., Hermans, M.J.M., Richardson, I.M., 2021. The effects of process parameters on melt-pool oscillatory behaviour in gas tungsten arc welding. *J. Phys. D Appl. Phys.* 54 (27), 275303. <https://doi.org/10.1088/1361-6463/abf808>.
- Ebrahimi, A., Kleijn, C.R., Richardson, I.M., 2019. The influence of surface deformation on thermocapillary flow instabilities in low Prandtl melting pools with surfactants. *Proceedings of the 5th World Congress on Mechanical, Chemical, and Material Engineering*. Avestia Publishing. <https://doi.org/10.11159/htff19.201>.
- Ebrahimi, A., Kleijn, C.R., Richardson, I.M., 2019. Sensitivity of numerical predictions to the permeability coefficient in simulations of melting and solidification using the enthalpy-porosity method. *Energies* 12 (22), 4360. <https://doi.org/10.3390/en12224360>.
- Ebrahimi, A., Kleijn, C.R., Richardson, I.M., 2021. Numerical study of molten metal melt pool behaviour during conduction-mode laser spot melting. *J. Phys. D Appl. Phys.* 54, 105304. <https://doi.org/10.1088/1361-6463/abca62>.
- Ebrahimi, A., Kleijn, C.R., Richardson, I.M., 2021. A simulation-based approach to characterise melt-pool oscillations during gas tungsten arc welding. *Int. J. Heat Mass Transf.* 164, 120535. <https://doi.org/10.1016/j.ijheatmasstransfer.2020.120535>.
- Ebrahimi, A., Sattari, M., Bremer, S.J.L., Luckbauer, M., Willem, R.B.E., Römer, G., Richardson, I.M., Kleijn, C.R., Hermans, M.J.M., 2022. The influence of laser characteristics on internal flow behaviour in laser melting of metallic substrates. *Mater. Des.* 214, 110385. <https://doi.org/10.1016/j.matdes.2022.110385>.
- Ferreira, J., Branco, C., 1991. Influence of misalignment on the fatigue strength of butt welds. *Int. J. Fatigue* 13 (5), 405–409. [https://doi.org/10.1016/0142-1123\(91\)90597-r](https://doi.org/10.1016/0142-1123(91)90597-r).
- Flint, T.F., Smith, M.C., Shanthraj, P., 2021. Magneto-hydrodynamics of multi-phase flows in heterogeneous systems with large property gradients. *Sci. Rep.* 11 (1) <https://doi.org/10.1038/s41598-021-97177-8>.
- Hejripour, F., Helenbrook, B.T., Valentine, D.T., Aidun, D.K., 2019. Mass transport and solidification phenomenon in dissimilar metals arc welding. *Int. J. Heat Mass Transf.* 144, 118703. <https://doi.org/10.1016/j.ijheatmasstransfer.2019.118703>.
- Hirt, C.W., Nichols, B.D., 1981. Volume of fluid (VOF) method for the dynamics of free boundaries. *J. Comput. Phys.* 39 (1), 201–225. [https://doi.org/10.1016/0021-9991\(81\)90145-5](https://doi.org/10.1016/0021-9991(81)90145-5).
- Issa, R.I., 1986. Solution of the implicitly discretised fluid flow equations by operator-splitting. *J. Comput. Phys.* 62 (1), 40–65. [https://doi.org/10.1016/0021-9991\(86\)90099-9](https://doi.org/10.1016/0021-9991(86)90099-9).
- Jaques, A., 1988. Thermophysical Properties of Argon. Technical Report FNAL-TM-1517. Illinois, United States.
- Kholoud, M.J., Akbari, M., 2021. Numerical investigation of molten pool dimension, temperature field and melting flow during pulsed laser welding of Ti-6Al-4V alloy sheets with different thicknesses. *J. Laser Appl.* 33 (3) <https://doi.org/10.2351/7.0000436>.
- Kromer, R., Gorny, C., Gruhier, E., Guen, E.L., Arvieu, C., Lacoste, E., 2023. Absorptivity measurement of solid and powder bed under IR laser beam. *Opt. Laser Technol.* 157, 108508. <https://doi.org/10.1016/j.optlastec.2022.108508>.
- Lancaster, J.F., 1986. The Physics of Welding. International Series on Materials Science of Technology, 2nd ed. Pergamon Press, Oxford, UK. ISBN 0080340768
- Li, Z., Rostam, K., Panjehpour, A., Akbari, M., Karimipour, A., Rostami, S., 2020. Experimental and numerical study of temperature field and molten pool dimensions in dissimilar thickness laser welding of Ti6Al4V alloy. *J. Manuf. Process.* 49, 438–446. <https://doi.org/10.1016/j.jmapro.2019.11.024>.
- Li, Z., Yu, G., He, X., Tian, C., Li, S., Li, H., 2022. Probing thermocapillary convection and multisolute dilution in laser welding of dissimilar miscible metals. *Int. J. Therm. Sci.* 172, 107242. <https://doi.org/10.1016/j.ijthermalsci.2021.107242>.
- Liang, R., Luo, Y., 2017. Study on weld pool behaviors and ripple formation in dissimilar welding under pulsed laser. *Opt. Laser Technol.* 93, 1–8. <https://doi.org/10.1016/j.optlastec.2017.01.029>.
- Lindgren, L.-E., Lundbäck, A., 2018. Approaches in computational welding mechanics applied to additive manufacturing: review and outlook. *Comptes Rendus Mécanique* 346 (11), 1033–1042. <https://doi.org/10.1016/j.crme.2018.08.004>.
- Lotsberg, I., 2009. Stress concentrations due to misalignment at butt welds in plated structures and at girth welds in tubulars. *Int. J. Fatigue* 31 (8-9), 1337–1345. <https://doi.org/10.1016/j.ijfatigue.2009.03.005>.
- Patankar, S.V., 1980. Numerical Heat Transfer and Fluid Flow, 1st ed. Taylor & Francis Inc. ISBN 0891165223
- Patterson, T., Hohanadel, J., Sutton, S., Panton, B., Lippold, J., 2021. A review of high energy density beam processes for welding and additive manufacturing applications. *Welding World* 65 (7), 1235–1306. <https://doi.org/10.1007/s40194-021-01116-0>. Release 19.2. ANSYS Fluent. URL <https://www.ansys.com/>.
- Tang, F., Wei, Y., Qian, L., Tang, Y., Chen, J., 2023. Asymmetry of keyhole and weld pool geometry in PLBW of tailor-welded steel sheets with edge misalignment: Numerical modeling and experimental validation. *Opt. Laser Technol.* 161, 109205. <https://doi.org/10.1016/j.optlastec.2023.109205>.
- Tsirkas, S.A., Papanikos, P., Kermanidis, T., 2003. Numerical simulation of the laser welding process in butt-joint specimens. *J. Mater. Process. Technol.* 134 (1), 59–69. [https://doi.org/10.1016/s0924-0136\(02\)00921-4](https://doi.org/10.1016/s0924-0136(02)00921-4).
- Ubbink, O., 1997. Numerical prediction of two fluid systems with sharp interfaces. Imperial College London (University of London), London, United Kingdom. PhD dissertation. URL <http://hdl.handle.net/10044/1/8604>
- Walther, D., Schmidt, L., Schrick, K., Junger, C., Bergmann, J.P., Notni, G., Mäder, P., 2022. Automatic detection and prediction of discontinuities in laser beam butt welding utilizing deep learning. *J. Adv. Joining Process.* 6, 100119. <https://doi.org/10.1016/j.jajp.2022.100119>.
- Wei, H.L., Mukherjee, T., Zhang, W., Zuback, J.S., Knapp, G.L., De, A., DeRoy, T., 2021. Mechanistic models for additive manufacturing of metallic components. *Prog. Mater. Sci.* 116, 100703. <https://doi.org/10.1016/j.pmatsci.2020.100703>.
- Wei, H.L., Pal, S., Manvatkar, V., Lienert, T.J., DeRoy, T., 2015. Asymmetry in steel welds with dissimilar amounts of sulfur. *Scr. Mater.* 108, 88–91. <https://doi.org/10.1016/j.scriptamat.2015.06.024>.
- Xia, J., Jin, H., 2016. Numerical study of welding simulation and residual stress on butt welding of dissimilar thickness of austenitic stainless steel. *Int. J. Adv. Manuf. Technol.* 91 (1-4), 227–235. <https://doi.org/10.1007/s00170-016-9738-2>.
- Xiao, M., Gao, C., Tan, C., Zhao, Y., Liu, H., Yang, J., 2021. Experimental and numerical assessment of interfacial microstructure evolution in dissimilar Al/steel joint by diode laser welding-brazing. *Optik* 245, 167706. <https://doi.org/10.1016/j.ijleo.2021.167706>.

- Xu, H., Guo, X., Lei, Y., Lin, J., Fu, H., Xiao, R., Huang, T., Shin, Y.C., 2019. Welding deformation of ultra-thin 316 stainless steel plate using pulsed laser welding process. *Opt. Laser Technol.* 119, 105583. <https://doi.org/10.1016/j.optlastec.2019.105583>.
- Ye, J., Khairallah, S.A., Rubenchik, A.M., Crumb, M.F., Guss, G., Belak, J., Matthews, M. J., 2019. Energy coupling mechanisms and scaling behavior associated with laser powder bed fusion additive manufacturing. *Adv. Eng. Mater.* 21 (7), 1900185. <https://doi.org/10.1002/adem.201900185>.
- Zhang, X., Li, L., Chen, Y., Zhu, X., Ji, S., 2019. Numerical simulation analysis of dual-beam laser welding of tailored blanks with different thicknesses. *Metals* 9 (2), 135. <https://doi.org/10.3390/met9020135>.
- Zhang, Y.M., Yang, Y.-P., Zhang, W., Na, S.J., 2020. Advanced welding manufacturing: a brief analysis and review of challenges and solutions. *J. Manuf. Sci. Eng.* 142 (11) <https://doi.org/10.1115/1.4047947>.
- Zhou, J., Tsai, H.L., 2005. 2 - Welding heat transfer. *Process. Mech. Welding Residual Stress Distortion* 32-98. <https://doi.org/10.1533/9781845690939.1.32>.